Proceedings of the
47th IEEE Conference on Decision and Control
Cancun, Mexico, Dec. 9-11, 2008



# Tracking a magnetic nanoparticle in 3-D with a magnetic force microscope

Dimitar Baronov and Sean B. Andersson

*Abstract*— **In this paper we introduce a scheme for tracking a magnetic nanoparticle in 3-D with the tip of a magnetic force microscope. The stray magnetic field of the magnetic particle induces a shift in the phase of oscillation of the tip of the MFM. We present a feedback control law which translates the measurement of this phase shift into actuator commands to the MFM and prove that the trajectory of the tip converges to a neighborhood of the magnetic particle. This geometric control law depends only on the derivative of the potential along the trajectory of the tip and in particular does not rely on any detailed prior knowledge about the nanoparticle. The results of simulation studies are shown to illustrate the algorithm.**

## I. Introduction

In this paper we develop a novel technique for tracking a magnetic nanoparticle in three dimensions with the tip of a magnetic force microscope (MFM). Such particles can be selectively bound to a wide-variety of biological molecules of interest [1]. Studying the dynamics of a bound nanoparticle therefore reveals information on the dynamics of the molecule itself. Motivated by this ability, we introduce a feedback control law which steers the tip of the MFM to remain in a neighborhood of a single magnetic particle. This works builds upon a previous effort of the authors [2]. The contribution of the present paper is a new algorithm which does not depend on detailed *a priori* information about the nanoparticle and which is designed to operate in 3-D.

The MFM is a scanning force microscope (SFM) utilizing a ferromagnetic probe as a tip. The resolution and sensitivity of the images that can be obtained depend largely on the geometric and magnetic properties of the probe. Spatial resolution on the order of 100 nm is readily achievable [3] and more recently researchers have achieved resolution as fine as 10 nm [4], [5]. As with all SFM technologies, images are built pixel-by-pixel using the standard raster-scan pattern. The standard approach to studying dynamic phenomena using SFM is to acquire a series of images and then post-process them to extract information about the motion of objects of interest. The temporal resolution is determined by the achievable frame rate. Because each image typically takes on the order of seconds to minutes to acquire, this approach is limited in terms of its applicability.

There are many systems in molecular biology and in engineered nano-systems with dynamics much faster than these frame rates. Most approaches for improving the temporal resolution center on improving the speed at which the tip can be moved while keeping the quality of the image high. Despite recent success in this area, e.g. [6]-[8], the rate of image acquisition remains much slower than the rate of motion of many biological molecules.

An alternative approach to improving the temporal resolution is to reduce the number of sampling points. Such non-raster techniques take advantage of *a priori* knowledge of the sample to steer the tip to points where sampling is needed and avoid regions where it is not [9]-[11]. The algorithm developed here uses the measurements obtained by the tip in real-time to steer the tip so that it tracks the motion of the magnetic nanoparticle. Information about position and motion is then obtained directly rather than extracted from a sequence of images. The temporal resolution is driven by the convergence rate of the control law and ultimately by the performance bounds of the actuators.

The control law proposed here is related to a broader class of work of one of the authors [12], [13]. The core application is one of studying a spatially-distributed phenomenon using a point-like or short-range mobile sensor. The limited information that can be acquired at any single instant of time requires "smart" techniques to increase the efficiency and the speed with which these phenomena are evaluated and their evolution tracked. In the large scale, there is an extensive volume of literature describing control laws which reactively achieve these objectives [14]-[17]. In many cases these approaches rely on a group of mobile sensors and do not translate well to applications in SFM where only a single sensor (the tip of the microscope) is available. The techniques described in [12], [13] are well suited for this challenge, since they rely on input from a single sensor and on geometrical features of the potential field that are well-behaved to scaling.

## II. MFM - theoretical background

This section lays out the model of the physical phenomena that enable the tracking of a magnetized particle by an MFM. A version of this section appeared previously in [2].

In magnetic force microscopy, the cantilever is excited with a low-amplitude sinusoidal drive signal and the tip is then brought near the sample. Interactions between the magnetized tip and the magnetic particle lead to a shift in the phase of the tip oscillation. In the conventional mode of operation, the tip is scanned at a constant vertical displacement over the sample surface. The image of the phase shift then reveals details of the underlying magnetic field. As discussed in Section III, we will utilize this phase shift in a feedback control law aimed at tracking the motion of the particle.

This work was supported in part by ODDR&E MURI07 Program Grant Number FA9550-07-1-0528, by the National Science Foundation through ITR Program Grant No. DMI-0330171 and through IDBR Program Grant No. DBI-0649823, all to Boston University.

D. Baronov and S.B. Andersson are with the Department of Mechanical Engineering, Boston University, Boston, MA, 02215. {baronov,sanderss}@bu.edu

978-1-4244-3124-3/08/$25.00 ©2008 IEEE

### A. Force to phase model

In the following we derive the dependence of the phase shift on the external force applied to the cantilever. ( See also [3].) The geometry of the tip-particle system is illustrated in Fig. 1. The tip motion is given with respect to a fixed coordinate frame whose $(x, y)$ axes lie in the sample plane. The amplitude of oscillation, typically between 10-100 Å, is small with respect to the length of the cantilever [18]. Therefore it is assumed that the tip motion is purely in the $z$ direction. Under this assumption, the dynamics of the tip can be simplified as a damped harmonic oscillator, which yields:

$$\frac{d^2 z_{tip}}{dt^2} + \frac{\omega_0}{Q}\frac{dz_{tip}}{dt} + \omega_0^2(z_{tip} - z_0) = \delta_0\omega_0^2\cos(\omega t) + \frac{\omega_0^2}{k}F_z, \tag{1}$$

where $z_{tip}$ is the distance between the probe and the sample plane, $z_0$ is the probe-sample distance at zero oscillation amplitude, $\delta_0$ is the amplitude of displacement at the clamped end of the cantilever, $k$ is the spring constant, $\omega_0$ is the natural frequency, and $Q$ is the quality factor of the oscillation. The force $F_z$ is the magnetic force $\mathbf{F} \in \mathbb{R}^3$ projected onto the $z$ axis.

If $F_z = 0$, the system is completely linear and its phase response yields:

$$\phi = \tan^{-1}\left(\frac{\omega\omega_0}{Q\left(\omega_0^2 - \omega^2\right)}\right). \tag{2}$$

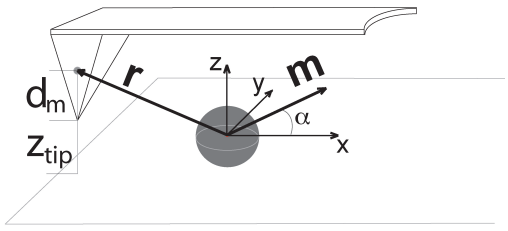


Fig. 1. MFM setup. Here $\mathbf{r}$ is the position vector of the effective dipole moment relative to the particle center, $d_m$ is the distance of the effective magnetic dipole moment relative to the end of the tip, $z_{tip}$ is the distance from the end of the tip to the sample plane containing the center of the magnetic particle, $\mathbf{m}$ is the particle's magnetization vector, and $\alpha$ is the angle between the $x$ axes and $\mathbf{m}$, given $\mathbf{m}$ lies in the $\{x, z\}$ plane.

Due to the small amplitude of the oscillation, we linearize the interaction force around a nominal displacement $z_0$:

$$F_z\left(z_{tip}\right) = F_z\left(z_0, 0\right) + \left.\frac{dF_z}{dz}\right|_{z=z_0}\left(z_{tip} - z_0\right).$$

Introducing the linearized term in (1) leads to a change in the natural frequency,

$$\tilde{\omega}_0 = \omega_0\sqrt{1 - \frac{1}{k}F_z'}, \tag{3}$$

which in turn changes the phase response of the system:

$$\tilde{\phi} = \tan^{-1}\left(\frac{\omega\tilde{\omega}_0}{Q\left(\tilde{\omega}_0^2 - \omega^2\right)}\right). \tag{4}$$

Thus the magnetic field of the particle induces a phase shift $\Delta\phi = \phi - \tilde{\phi}$ in the frequency of the oscillation. The sensitivity of this response is maximized when the tip is driven near its original natural frequency $\omega = \omega_0$. From (2), this corresponds to $\phi = \frac{\pi}{2}$. Then, setting $\omega = \omega_0$ in (4) gives:

$$\Delta\phi \;=\; \tan^{-1}\left(-\frac{Q\frac{1}{k}F_z'}{\sqrt{1 - \frac{1}{k}F_z'}}\right).$$

### B. Magnetic force model

The magnetic force arising from the tip-particle interaction can be described by a convolution integral [19]:

$$\mathbf{F}(\mathbf{r}_{tip}(t)) = \mu_0\int_{tip}\left(\mathbf{M}_{tip}(\mathbf{r}')\cdot\nabla_{\mathbf{r}_{tip}}\right)\mathbf{H}_s\left(\mathbf{r}_{tip} - \mathbf{r}'\right)d\mathbf{r}', \tag{5}$$

where $\mathbf{M}_{tip} \in \mathbb{R}^3$ is magnetization of the tip, $\mathbf{H}_s \in \mathbb{R}^3$ is the stray field of the sample and $\mathbf{r}_{tip}(t) \in \mathbb{R}^3$ is the position of the tip. The oscillation amplitude of the tip is very small with respect to the nominal separation of the tip and the sample, denoted by $\mathbf{r}_0$. Therefore, we assume that $\mathbf{r}_{tip}(t) = \mathbf{r}_0$.

To simplify the convolution integral, the MFM tip is usually abstracted as a point probe that is comprised of a magnetic monopole and/or a magnetic dipole [3], [20], [21]. It has been shown that to perform an unambiguous analysis of the MFM response, only one of these contributing terms should be used [21]. In the analysis that follows, we use the magnetic dipole model. This choice simplifies (5) to:

$$\mathbf{F}(\mathbf{r}_0) = \mu_0\left(\mathbf{m}\cdot\nabla\right)\mathbf{H}_s(\mathbf{r}_0 + \mathbf{r}_m), \tag{6}$$

where $\mathbf{m}$ is the effective dipole moment and $\mathbf{r}_m$ is its position relative to the end of the tip. (This notation is visualized in Fig. 1.) Assuming the MFM tip is magnetized such that the magnetization vector lies along the $z$ direction, (6) yields

$$F_z'(\mathbf{r}_0) \;=\; \frac{d}{dz}\left(\mathbf{F}\cdot\hat{\mathbf{z}}\right) = \mu_0 m_z\left.\frac{\partial^2 H_z}{\partial z^2}\right|_{\mathbf{r}=\mathbf{r}_0+\mathbf{r}_m}, \tag{7}$$

where $\mathbf{m} = \{0, 0, m_z\}^T$ and $\mathbf{r}_m = \{0, 0, d_m\}$. Note that both parameters characterizing the tip, $m_z$ and $d_m$, are unknown and are usually determined by fitting the model to experimental data [20], [21].

The magnetic beads that we intend to track are small, uniformly magnetized spheres. The stray magnetic field from such a particle is given by:

$$\mathbf{H}_s(\mathbf{r})_{r>a} = \frac{1}{4\pi}\left[-\frac{\mathbf{m}_s}{r^3} + \frac{3\left(\mathbf{m}_s\cdot\mathbf{r}\right)\mathbf{r}}{r^5}\right], \tag{8}$$

where $\mathbf{r}$ is a radius vector whose origin coincides with the center of the sphere, $a$ is the radius of the sphere and $\mathbf{m}_s$ is the equivalent magnetic moment of the sphere. The moment $\mathbf{m}_s$ depends both on the material magnetization, $M$, and the volume of the sphere:

$$\mathbf{m}_s = \frac{4}{3}\pi a^3 M\hat{\mathbf{n}}, \tag{9}$$

where $\hat{\mathbf{n}}$ is the unit vector specifying the orientation of the magnetization. Rearranging (9), (8) and (7) leads to the following expression for the derivative of the force:

$$F_z'(\mathbf{r_0}) = b\mathcal{S}(\mathbf{r}_0, d_m), \tag{10}$$

where the scale factor $b$ is equal to:

$$b = \frac{1}{3}\mu_0 m_z a^3 M, \tag{11}$$

and $\mathcal{S}$ is a function of the nominal position of the tip and the displacement of the equivalent dipole moment from the tip given by:

$$\mathcal{S}(\mathbf{r}_0, d_m) = \frac{\partial^2}{\partial z^2}\left[-\frac{\hat{\mathbf{n}}}{r^3} + \frac{3\left(\hat{\mathbf{n}}\cdot\mathbf{r}\right)\mathbf{r}}{r^5}\right]\cdot\hat{\mathbf{z}}\Bigg|_{\mathbf{r}=\mathbf{r}_0+\{0,0,d_m\}^T}$$

where $r$ is the Euclidean length of $\mathbf{r}$.

To analyze the geometry of the map $\mathcal{S}$, it can be assumed without loss of generality that the direction of the magnetization vector of the sphere $\hat{\mathbf{n}}$ lies in the $\{x, z\}$ plane. Then, setting $\alpha$ to be the angle between $\hat{\mathbf{n}}$ and the $\{x, y\}$ plane (Fig. 1) gives the following expression for $\mathcal{S}$:

$$\begin{aligned}\mathcal{S} = \quad &- \quad \frac{3}{4\pi}\frac{5x_0 z(3r_{xy} - 4z^2)}{r^9}\cos\alpha + \\ &+ \quad \frac{3}{4\pi}\frac{3r_{xy}^4 - 24r_{xy}^2 z^2 + 8z^4}{r^9}\sin\alpha \end{aligned} \tag{12}$$

Here $z = z_0 + d_m$ and $r_{xy}$ is the Euclidian length of the projection of $\mathbf{r} = \{x_0, y_0, z\}^T$ into the $\{x, y\}$ plane, $\mathbf{r}_{xy}$.

Inserting (12) into (10) gives $F_z'$ which in turn yields the phase shift from (5). Fig. 2 shows a simulated raster scan image of the phase shift in the region around the particle, based on the developed model for three different values of angle $\alpha$ and $z_0 = 50$ nm. For $\alpha = 0$, corresponding to the magnetization vector of the particle lying in the sample plane, there are two distinguishing regions, one determined by repelling forces, the other by attracting. As the magnetization vector rotates out of the sample plane, one of the poles becomes dominant at the expense of the other.

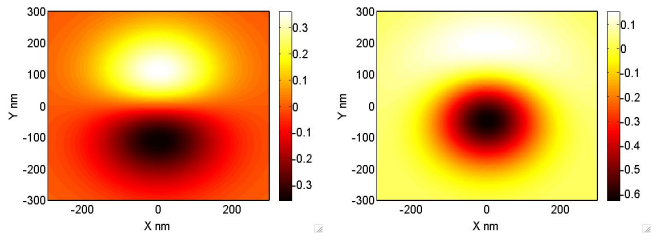


(a) $\alpha = 0$ (b) $\alpha = 45$ deg

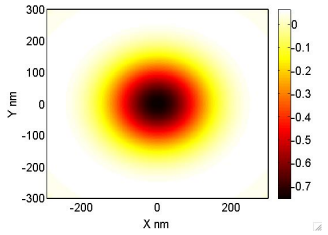


(c) $\alpha = 90$ deg

Fig. 2. The phase shift (degrees) for three different values of $\alpha$. The tip-sample separation was set to $z_0 = 50$ nm and the model parameters to: $Q = 180$, $k = 1$ N/m, $m_z = 5.1 \times 10^{-15}$ Am$^2$, $d_m = 300$ nm, $M = 480 \times 10^3$ A/m (the saturation magnetization of magnetite - $Fe_2 0_3$) and $a = 25$ nm. The values for $m_z$ and $d_m$ are from experiments in [20].

To quantify the noise entering the measurement system, we assume that its main component is due to thermal motion of the cantilever [22]. The standard deviation of this noise is given by

$$\sigma_{F_z'} = \frac{1}{\delta_{rms}}\sqrt{\frac{2kk_bTB}{\omega_0 Q}}, \tag{13}$$

where $\delta_{rms}$ is the root mean-square amplitude of the tip, $k_b$ is the Boltzmann's constant, $T$ is the ambient temperature and $B$ is the bandwidth of the measurements. Using the linearization of (5), we can propagate the noise into the phase shift to find the standard deviation in the measurement of the phase shift is given by:

$$\sigma_{\Delta\phi} = \left.\frac{d\Delta\phi}{dF_z'}\right|_{F_z'=0}\sigma_{F_z'} = \frac{Q}{k}\sigma_{F_z'}. \tag{14}$$

## III. Tracking control

Our goal is to develop a feedback control law which steers the tip to an arbitrarily small neighborhood around the particle. Relative motion between the tip and the sample in an MFM is commonly achieved using piezo-electric actuators. These systems exhibit a variety of interesting and important dynamic effects, including nonlinearities such as creep and hysteresis. There is, however, a large body of existing literature on efficient and effective controllers for these systems (see, e.g. [23], [7] and discussions in [8]). For the remainder of this paper, we will assume the existence of a low-level controller that compensates for the dynamics of the actuators and focus on trajectory determination. Under this assumption, the motion of the tip can be modeled as:

$$\dot{\mathbf{r}} = \begin{pmatrix} \dot{\mathbf{r}}_{xy} \\ \dot{z}_0 \end{pmatrix} = \mathbf{u} = \begin{pmatrix} u_x \\ u_y \\ u_z \end{pmatrix}, \tag{15}$$

where $u_x$, $u_y$ and $u_z$ are the available control inputs. In this work, we divide the controller into a planar $(x - y)$ component and a separate axial $(z)$ component.

### A. Tracking in the plane

Here, we assume that the particle and the tip evolve in two parallel planes at a constant nominal displacement $z_0$. For fixed $z_0$, it can be seen from (10) that $F_z' : \mathbb{R}^2 \to \mathbb{R}^1$. As a result, the phase shift $\Delta\phi$ can be abstracted as a scalar potential function:

$$\begin{aligned}\Delta\Phi(\cdot) : \mathbb{R}^2 \quad &\to \quad \mathbb{R}, \\ \mathbf{r}_{xy} \quad &\mapsto \quad \Delta\Phi(\mathbf{r}_{xy}),\end{aligned}$$

where $\Delta\phi(t) = \Delta\Phi\left(\mathbf{r}_{xy}\left(t\right)\right)$ with $\mathbf{r}_{xy}(\cdot)$ the trajectory of the tip.

The geometry of the field $\Delta\Phi\left(\mathbf{r}_{xy}\right)$ plays an important part in the control design. As discussed in Section II, the field has one or two extrema depending on the orientation of the magnetization vector of the particle. Therefore, by tracking an extremum, the particle itself can be tracked. In this perspective, a tracking control should navigate the tip through the potential and converge it to a neighborhood

around its extremum. The choice of which extremum to track is arbitrary and is determined purely by initial conditions.

In [12] [13], one of the authors introduced an algorithm for navigating a vehicle through an unknown potential field without directly estimating the gradient of the field. This was achieved through the introduction of nonholonomic constraints on the kinematics of the vehicle together with the choice of constant speed. In the MFM setup, this is equivalent to the control input in (15) having the form:

$$\begin{aligned} \mathbf{u} &= \begin{pmatrix} \cos(\theta) \\ \sin(\theta) \end{pmatrix} \\ \dot{\theta} &= \omega, \end{aligned} \tag{16}$$

where $\omega$ is function of both $\Delta\phi$ and $\frac{d\Delta\phi}{dt}$ and corresponds to a steering rate for the direction of the tip motion.

The level sets of $\Delta\Phi$ can be approximated as circles in a neighborhood near an extremum (Fig. 2). For the design of the tracking control, we exploit this characteristic of the potential function and formalize it with the following assumption.

*Assumption 1:* Let $\Delta\Phi^* = |\Delta\Phi(\mathbf{r}^*_{xy})|$ be the value of $\Delta\Phi(\mathbf{r}_{xy})$ at its extremum. Then for some positive constant $\beta$, there exists a neighborhood

$$\Omega = \{\mathbf{r}_{xy} \in \mathbb{R}^2 \,|\Delta\Phi^* - \beta \leq |\Delta\Phi\left(\mathbf{r}_{xy}\right)|\,\}$$

such that

$$\|\nabla\left(\Delta\Phi\right)\| \geq \sigma, \quad \mathbf{r}_{xy} \in \Omega, \tag{17}$$

for a given $\sigma > 0$ and such that

$$\sup_{\mathbf{r_{xy}} \in \Omega} \left|\Delta\Phi(\mathbf{r}_{xy}) - f_p\left(\left\|\mathbf{r}_{xy} - \mathbf{r}^*_{xy}\right\|\right)\right| \leq \epsilon, \tag{18}$$

where $f_p$ is a radial function and $\epsilon$ a small positive constant. ■

The tracking control derived below relies explicitly on (18) and (17). To ensure these assumptions are met, the control action will consist of two consecutive phases. The first is a search in which the tip is scanned over the sample until it detects a phase shift $\Delta\phi \geq \beta$ for a given $\beta$ large enough so that the tip is in a region for which the radial approximation holds. The second phase is the tracking control (described below) in which the tip converges to a circular orbit around the extremum and with a pre-specified radius.

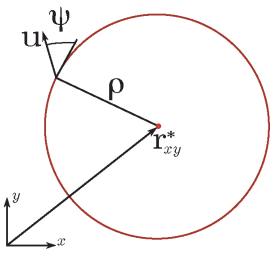


Fig. 3. The motion of the tip in terms of $\psi$ and $\rho$

Following the radial potential field assumption, the motion of the tip can be expressed in coordinates directly related to the potential. We choose here the radius $\rho = \left\|\mathbf{r}_{xy} - \mathbf{r}^*_{xy}\right\|$, defined as the distance between the current position of the tip and the nearest extremum, and the angle $\psi$, being the angle between the tangent to a level set and the heading of the tip (Fig. 3). Under the nonholonomic constraints introduced in (16), it can be shown [13] that in the chosen coordinates, the system evolution is:

$$\begin{aligned} \dot{\rho} &= \sin\psi \\ \dot{\psi} &= \omega + \frac{1}{\rho}\cos\psi. \end{aligned} \tag{19}$$

Moreover, in this coordinate system $\frac{d\Delta\phi}{dt}$ yields:

$$\frac{d\Delta\phi}{dt} = -\|\nabla\left(\Delta\Phi\right)\|\sin\psi.$$

Therefore, under the chosen control, (19) is an autonomous system where the geometry of the field manifests itself through the magnitude of its gradient $\|\nabla\left(\Delta\Phi\right)\|$ and the curvature of the level sets, $\frac{1}{\rho}$, both evaluated at the position of the tip. Neither the gradient nor the curvature can be directly measured. Nevertheless, the theorem below establishes a control law such that the tip trajectory converges to $\rho(t) \leq \rho_c$ for a given $\rho_c > 0$.

*Theorem 1:* Define the sets

$$\begin{aligned} B &= \left\{\mathbf{r}_{xy} \in \mathbb{R}^2 \left| \frac{\rho}{\rho_0} - \ln\frac{\rho}{\rho_0} \leq 2 \right.\right\}, \\ D &= \left\{\{\rho,\psi\}^T \in \mathbb{R}^2 \left| \frac{\rho}{\rho_0} - \ln\frac{\rho}{\rho_0} + \cos\psi \leq 1 \right.\right\}, \end{aligned}$$

for some $\rho_0 > 0$ and let Assumption 1 hold. If $B \subseteq \Omega$, then under the control law defined by:

$$\omega = \frac{1}{\rho_0}\left(1 - K\frac{d}{dt}|\Delta\phi|\right), \tag{20}$$

where

$$K \geq \frac{1}{\sigma}\sup_{\{\rho,\psi\}\in D}\left(\frac{1}{\rho}\sin\psi\right), \tag{21}$$

the tip trajectory satisfies

$$\left\|\mathbf{r}_{xy}(t) - \mathbf{r}^*_{xy}\right\| \to \rho_0, \tag{22}$$

as $t \to \infty$, given that $\{\rho(0), \psi(0)\}^T \in D$.

*Proof:* The candidate Lyapunov function is:

$$V(\rho,\psi) = \frac{\rho}{\rho_0} - 1 - \ln\frac{\rho}{\rho_0} + 1 + \cos\psi. \tag{23}$$

Note that $\frac{\rho}{\rho_0} - 1 - \ln\frac{\rho}{\rho_0} > 0$ for $\rho \neq \rho_0$ and is unbounded. Therefore, the function will be positive definite in the interval $\psi \in [\frac{\pi}{2}, 3\frac{\pi}{2}]$, or $D = \{\{\rho,\psi\}^T \in \mathbb{R}^2 | V(\rho,\psi) \leq 1\}$ will be a compact set. Taking the derivative on the trajectory of the system yields:

$$\begin{aligned} \dot{V} &= -\frac{1}{\rho_0}\sin^2\psi\left(MK - \frac{1+\cos\psi}{\sin\psi}\frac{1}{\rho}\right) \leq & (24) \\ &\leq -\frac{1}{\rho_0}\sin^2\psi\left(MK - |\sin\psi|\frac{1}{\rho}\right). & (25) \end{aligned}$$

Since $\rho \in D$ implies $\rho \in B$ it follows that $M \geq \sigma$. Therefore, choosing $K$ according to (21) guarantees that

$\dot{V} \leq 0$. In such case, the LaSalle's invariance principal guarantees the system to asymptotically converge to the equilibrium $\rho = \rho_0, \psi = \pi$, which proves (22). ■
(For a less conservative estimation of the invariant set for (19) with control laws of the type (20) see [13].)

We note that in previous work [2], we used a similar approach to develop a control law to track a given level set $\Delta\Phi = const$ near the extremum. That law required knowledge of model parameters that in general are difficult to determine. The control introduced here relies only on the measured phase shift and its derivative. Explicit parameter values are not needed, though an estimate of the value of $\beta$ is required to ensure Assumption 1 is satisfied and a value of $\rho_0$ such that the tip stays in the set $\Omega$.

### *B. Tracking in three dimensions*

To develop a tracking controller in the axial direction, we first define the scalar potential $\Delta\tilde{\Phi} : \mathbb{R}^3 \rightarrow \mathbb{R}$ in an analogous fashion to the planar potential in the previous section. We also extend Assumption 1 to $\mathbb{R}^3$ as follows:

*Assumption 2:* Let $\mathbf{r} = 0$ be the position of the particle's center. Then there exists a neighborhood $\tilde{\Omega} = \{\mathbf{r} \in \mathbb{R}^3 : z > 0 \,\big|\, |\Delta\tilde{\Phi}(\mathbf{r})| > \tilde{\beta}\}$ such that

$$\left\| \nabla \left( \Delta\tilde{\Phi} \right) \right\| \geq 0, \quad \mathbf{r} \in \tilde{\Omega}. \tag{26}$$

and

$$\sup_{\mathbf{r} \in \tilde{\Omega}} \left| \Delta\tilde{\Phi}(\mathbf{r}) - \tilde{f}_p \left( \|\mathbf{r}\| \right) \right| \leq \epsilon, \tag{27}$$

where $f_p$ is a radial function $\epsilon$ is a small positive constant.

Note that this assumption guarantees that for any fixed displacement $z_0$ between the particle center and the tip, the extremum of $\Delta\tilde{\Phi}(\mathbf{r})$ will be achieved for $\mathbf{r}_{xy} = 0$. Then, with $\rho$ and $\psi$ as before, we can write for the tracking system the following equations:

$$\begin{aligned} \dot{\rho} &= \sin\psi \\ \dot{\psi} &= \omega + \frac{1}{\rho}\cos\psi \\ \dot{z}_0 &= v, \end{aligned} \tag{28}$$

where $v$ is the vertical control of the tip. Note, that in this case:

$$\frac{d\tilde{f}_p}{dt} = -\left\| \nabla_{xy} \left( \Delta\tilde{\Phi} \right) \right\| \sin\psi + \frac{\partial \Delta\tilde{\Phi}}{\partial z} v. \tag{29}$$

*Theorem 2:* Define the constant $C$ as:

$$C = |\tilde{f}_p(\rho_0^2 + z_d)| > \tilde{\beta}. \tag{30}$$

for a given $z_d > 0$. Then there exists a neighborhood $\mathcal{B} \subset \mathbb{R}^2$ of $Z_0 = \{\rho = \rho_0, \psi = \pi, z_0 = z_d\}$, such that under the control law:

$$\omega = \frac{1}{\rho_0}\left(1 - K\frac{d}{dt}|\Delta\phi|\right), v = K_z(|\Delta\phi| - C), K, K_z > 0, \tag{31}$$

the system (28) converges to $Z_0$, for all $\forall Z(t) \in \mathcal{B}$.

*Proof:* Linearizing (28) around $Z_0$ under the control (31) yields:

$$\frac{d}{dt}\begin{bmatrix} \delta\rho \\ \delta\psi \\ \delta z \end{bmatrix} = A \begin{bmatrix} \delta\rho \\ \delta\psi \\ \delta z \end{bmatrix},$$

where

$$A = \begin{bmatrix} 0 & -1 & 0 \\ \frac{1}{\rho_0^2} - \frac{K_z K M_z M_{xy}}{\rho_0} & -\frac{K}{\rho_0} M_{xy} & -\frac{K K_z}{\rho_0} M_z^2 \\ -K_z M_{xy} & 0 & -K_z M_z \end{bmatrix}.$$

Here $M_{xy} = \left\| \nabla_{xy} \left( \Delta\tilde{\Phi} \right) \right\| > 0$ and $M_z = -\frac{\partial |\Delta\tilde{\Phi}|}{\partial z}$. Under the model in Section II, the magnitude of the force increases as the tip becomes closer to the particle. Therefore it can be verified that the linearized system matrix is Hurwitz. ■
Note, that the convergence of (28) to $Z_0$ corresponds to the tip converging to circular trajectory in the horizontal plane $z_0 = z_d$.

## IV. Numerical simulations

In this section, we describe a set of simulation studies of the proposed tracking scheme. The simulations consider a 100 nm diameter particle and include a model of thermal noise in the measurements. Parameter values were chosen as in Fig. 2 in Section II. Note that the the primary effect of different size particles is a change in the magnetic moment and thus the signal-to-noise ratio in the measurements.

The simulations take into account that the actual control should be implemented in the discrete domain. We assume that the control action is piece-wise constant, $\omega(t) = \text{const}$, $v(t) = \text{const}$, $t \in [t_k, t_{k+1})$, where $t_k$ corresponds to the update time of the controller. We take the interval $t_{k+1} - t_k$ to be equal to $\frac{1}{B}$, where $B$ is the bandwidth of the measurements. For the purposes of these simulations, the bandwidth was set to 300 Hz. The parameter values in the control law described in Section III were taken to be $\rho_0 = 60$ nm, $K = 100$, and $K_z = 12$. The horizontal distance which the tip travels between two consecutive updates is $d_{tip} = 10$ nm, which corresponds to $\|\dot{\mathbf{r}}_{xy}\| = 3\mu$m/s. The desired vertical displacement between the tip and the particle was set to $z_d = 90$ nm.

We considered first a fixed particle. Fig. 4(a) depicts the planar projection of the trajectory of the tip for a fixed particle, overlaid on a phase surface image corresponding to fixed $z_0 = 90$ nm. It can be verified by the figure that the horizontal component of the trajectory converges to the desired radius $\rho_0 = 60$ nm. Fig. 4(b) shows how $z_0$ varies with time. The tip begins initially at 150 nm above the center of the particle (or 100 nm above the surface) and then converges within 0.2 s (60 samples) to 90 nm above the particle center. The effect of noise on the trajectory can clearly be seen in the figure.

We then considered a particle moving with a speed of 0.6 $\mu$m/s in the plane and -0.15 $\mu$m/s in the axial direction. The resulting trajectory in the plane is shown in Fig. 5(a)-(c) at three snapshots in time. The image on the background corresponds to an MFM phase image at the current the tip - particle vertical separation. The vertical trajectory is shown

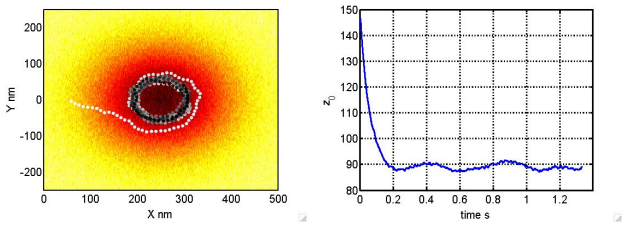


(a) Planar trajectory (b) Vertical trajectory

Fig. 4. The trajectory of the tip for a static particle. (a) Planar trajectory.Trajectory colors correspond to time with the most recent points depicted in black. The trajectory is overlaid on an MFM phase image at a tip-sample separation of 90 nm. The tip converges to a nearly circular trajectory with a radius of 60 nm. Noise in the measurements gives rise to variations in the trajectory. (b) Vertical trajectory. After 0.2 s (60 samples) the axial component has converged to the desired tip-sample separation.

in Fig. 5(d). Three distinct phases of the tip motion can be observed. In the first, the tip engages the particle and moves rapidly in the $z$ direction, following a spiral-like trajectory. In the transition stage the tip converges to a neighborhood of the particle. The final steady state phase corresponds to stable tracking. The background MFM phase image illustrates the improvement in the signal-to-noise ratio as the tip approaches the particle.

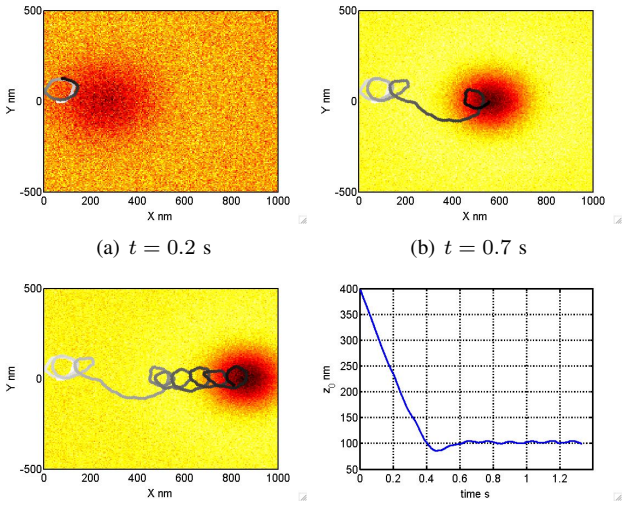


(a) $t = 0.2$ s (b) $t = 0.7$ s

(c) $t = 1.2$ s (d) Vertical trajectory

Fig. 5. Tracking a moving particle with velocity $V = 0.62\ \mu m/s$. (a-c) Snapshots of the planar trajectory of the tip. Colors correspond to time with the most recent points in black. (d) The vertical separation of the particle's center and the tip as function of time for a moving particle.

## V. Conclusions

In this paper we proposed a novel approach to study the dynamics of single molecules through the use of tracking. While experimental study is needed, simulation studies were shown that indicate effective tracking in a practical system can be achieved.

## References

[1] Q. A. Pankhurst, J. Connolly, S. K. Jones, and J. Dobson, "Applications of magnetic nanoparticles in biomedicine," *Journal of Physics D: Applied Physics*, vol. 36, no. 13, pp. R167–R181, July 2003.

[2] D. Baronov, S. B. Andersson, and J. Baillieul, "Tracking a nanosize magnetic particle using a magnetic force microscope," in *Proceedings of the IEEE Conference on Decision and Control*, 2007, pp. 2445–2550.

[3] U. Hartmann, "Magnetic force microscopy," *Annu. Rev. Mater. Sci.*, vol. 29, no. 1, pp. 53–87, 1999.

[4] M. R. Kobischka and U. Hartmann, "Improving the lateral resolution of the MFM technique to the 10 nm range," *J. Magn. Magn. Mater.*, vol. 272-276, no. 3, pp. 2138–2140, May 2004.

[5] G. Yang, J. Tang, S. Kato, Q. Zhang, L. C. Qin, M. Woodson, J. Liu, J. W. Kim, P. T. Littlehei, C. Park, and O. Zhou, "Magnetic nanowire based high resolution magnetic force microscope probes," *Appl. Phys. Lett.*, vol. 87, no. 12, p. 123507, September 2005.

[6] G. Schitter, K. J. Åström, B. E. DeMartini, P. J. Thurner, K. L. Turner, and P. K. Hansma, "Design and modeling of a high-speed afm scanner," *IEEE Transactions on Control Systems Technology*, vol. 15, no. 5, pp. 906–915, September 2007.

[7] Y. Wu and Q. Zou, "Iterative control approach to compensate for both the hysteresis and the dynamics effects of piezo actuators," *IEEE Transactions on Control Systems Technology*, vol. 15, no. 5, pp. 936–944, September 2007.

[8] D. Y. Abramovitch, S. B. Andersson, L. Y. Pao, and G. Schitter, "A tutorial on the mechanisms, dynamics and control of atomic force microscopes," in *Proceedings of the American Control Conference*, 2007, pp. 3488–3502.

[9] S. B. Andersson, "Curve tracking for rapid imaging in AFM," *IEEE Transactions on Nanobioscience*, vol. 6, no. 4, pp. 354–361, 2007.

[10] P. I. Chang and S. B. Andersson, "Smooth trajectories for imaging string-like samples in afm: a preliminary study," in *Proceedings of the American Control Conference, to appear*, Seattle, WA, June 2008, pp. 3207–3212.

[11] S. B. Andersson and D. Y. Abramovitch, "A survey of non-raster scan methods with application to atomic force microscopy," in *Proceedings of the American Control Conference*, 2007, pp. 3516–3521.

[12] D. Baronov and J. Baillieul, "Reactvie exploration through following isolines in a potential field," in *Proceedings of the American Controls Conference*, 2007, pp. 2141–2146.

[13] ——, "Autonomous vehicle control for ascending/descending along a potential field with two applications," in *Proceedings of the American Controls Conference*, 2008, pp. 678–683.

[14] N. E. Leonard, D. A. Pawley, F. Lekien, R. Sepulchre, D. M. Fratantoni, and R. E. Davis, "Collective motion, sensor networks, and ocean sampling," *Proceedings of the IEEE*, vol. 95, no. 1, pp. 48–74, January 2007.

[15] F. Zhang and N. E. Leonard, "Generating contour plots using multiple sensor platforms," in *Proceedings of the IEEE Swarm Intelligence Symposium*, 2005, pp. 309–314.

[16] P. Orgen, E. Fiorelli, and N. E. Leonard, "Cooperative control of mobile sensor networks: Adaptive gradient climbing in a distributed environment," *IEEE Transactions on Automatic Control*, vol. 49, no. 8, pp. 1292–1302, August 2004.

[17] S. Martínez and F. Bullo, "Optimal sensor placement and motion coordination for target tracking," *Automatica*, vol. 42, no. 4, pp. 661–668, 2006.

[18] D. Rugar, H. J. Guethner, S. E. Lambert, J. E. Stern, I. McFadyen, and T. Yogi, "Magnetic force microscopy: General principles and applications to longitudanal recording media," *J. Appl. Phys.*, vol. 68, no. 3, 1990.

[19] R. Engel-Herbert, D. Schaadt, and T. Hesjedal, "Analytical and numerical calculation of the magnetic force microscopy response: A comparison," *J. Appl. Phys.*, vol. 99, no. 113905, June 2006.

[20] S. McVitie, R.P.Ferrier, J. Scott, G. White, and A. Gallagher, "Quantitative field measurements from magnetic force tips and comparison with point and extended charge models," *J. Appl. Phys.*, vol. 89, no. 7, April 2001.

[21] J. Lohau, S. Kirsch, A. Carl, G. Dumpich, and E. F. Wassermann, "Quantitative determination of effective dipole and monopole moments of magentic force microscopy tips," *J. Appl. Phys.*, vol. 86, no. 6, pp. 3410–3417, September 1999.

[22] D. P. E. Smith, "Limits of force microscopy," *Rev. Sci. Instrum.*, vol. 66, no. 5, pp. 3191–3195, May 1995.

[23] D. Croft, G. Shed, and S. Devasia, "Creep, hysteresis, and vibration compensation for piezoactuators: atomic force microscopy application," *Journal of Dynamic Systems, Measurement, and Control*, vol. 123, no. 1, pp. 35–43, March 2001.